Efficient Design Optimization of PMSM Drive Systems Using Improved Equivalent-Circuit-Based Loss Minimization Control

Lin Liu, *Student Member, IEEE,* Youguang Guo, *Senior Member, IEEE,* Wenliang Yin, *Member, IEEE,* Gang Lei, *Senior Member, IEEE,* Xiaodong Sun, *Senior Member, IEEE,* and Jianguo Zhu, *Senior Member, IEEE*

***Abstract*—During the lifecycle of an electric drive system, the electricity cost usually constitutes a dominant portion, leading to extensive research on improving the efficiency of such systems. This paper presents an efficient design optimization strategy for permanent magnet synchronous motor (PMSM) drive systems, cooperated with an improved loss minimization control, targeting to reduce the system power loss and improve the overall operating performances. Specifically, a generalized equivalent circuit model with a novel topology that considers rotating magnetization effects is first proposed to accurately predict the core loss of PMSMs under both no-load and loaded conditions. Moreover, after analyzing the copper and inverter losses, an integrated system-level loss model of the PMSM drive system is developed, based on which an improved loss minimization control is implemented through deriving the relationships among the electromagnetic torque, *d*-axis and *q*-axis currents. Then, the system-level optimization strategy that incorporates both the motor and control sides is presented, aiming to maximize the torque and efficiency and minimize the torque ripple and speed overshoot. Finally, a multi-level algorithm based on sensitivity analysis is employed to solve the multi-objective optimization models with reduced calculation costs. Extensive experimental and simulation verifications are demonstrated with a 20 kW interior PMSM drive system platform. Results show that the optimized drive system has promoted steady-state and dynamic behaviors, and the proposed loss minimization control can comprehensively reduce the system losses by about 3.25%.**

***Index Terms*—Electric drive system, permanent magnet synchronous motor (PMSM), loss minimization control, equivalent circuit model, system-level optimization, multi-level strategy, system loss model.**

I. Introduction

Designing and optimizing electric drive systems for enhanced performance and higher efficiency is urgent and significant, garnering considerable innovation investments and research focus [1]. While researchers have made substantial efforts to optimize permanent magnet (PM) synchronous motors (PMSMs) and drive systems, technical challenges in complex operating conditions for electric vehicle (EV) drive systems remain [2]. First, existing design optimization has predominantly employed single-objective approaches, and to fully exploit optimization benefits, a shift towards multi-objective optimization is crucial to achieving a balanced set of performances [3]-[4]. Furthermore, previous optimization methods have often focused on component-level enhancements, which may not always lead to the overall optimization of the entire drive system [1], [4]. Modern systems demand specific, integrated design and optimization to support multiple performance indicators effectively. Recent work has highlighted the strong interdependencies among components in electric drive systems and the advantages of optimizing the system as a whole, encompassing both the motor and controller [5]-[6]. Therefore, identifying optimal parameters for the entire system, rather than separately optimizing the motor and controller and then assembling them into their respective applications, holds great significance.

The design optimization of EV drive systems at system level typically involves two main parts, namely, the design analysis and the performance optimization [1]. For the design analysis, accurate loss calculation is crucial in efficiency optimization. Researchers have also conducted substantive works on the efficiency optimizations of various types of electric machines and drives [6]-[7]. However, the loss models in these achievements only include two main electromagnetic losses, i.e., motor core loss and copper loss, without enough consideration of the losses aroused by the control system, resulting in restrictions on system efficiency improvements.

More specifically, for the motor side, the computation of core losses can be rather intricate and challenging, primarily due to the nonlinear characteristics of core materials and the complex magnetic field distributions [8]-[9]. The use of the Bertotti model in finite element analysis (FEA) has proven effective for accurately calculating core loss [10]. However, FEA is time-consuming, particularly in the iterative design optimization of PMSMs with complex structures [6]. Recently, to lower computational expenses, alternative methods for calculating core loss based on analytical models have been suggested [11]-[12]. Among them, the equivalent circuit model (ECM) enables

Manuscript received December 22, 2023; revised May 2, 2024; accepted ** ****, 2024. This work was supported in part by the Australian Research Council under Discovery Grants DP120104305 and DP180100470. (*Corresponding author: Youguang Guo*)

L. Liu, Y. Guo, and G. Lei are with the School of Electrical and Data Engineering, University of Technology Sydney, NSW 2007, Australia (E-mails: Lin.Liu@student.uts.edu.au; Youguang.Guo-1@uts.edu.au; Gang.Lei@uts.edu.au).

W. Yin and J. Zhu are with the School of Electrical and Information Engineering, The University of Sydney, NSW 2006, Australia (E-mails: wenliang.yin@sydney.edu.au; jianguo.zhu@sydney.edu.au).

X. Sun is with Automotive Engineering Research Institute, Jiangsu University, Zhenjiang 212013, China (E-mail: xdsun@ujs.edu.cn).

engineers to streamline motor design and optimization. By fine-tuning the parameters, the ECM can consider multiple factors influencing core losses and accelerate the design process [13]. However, to the authors' knowledge, in the conventional ECMs for PMSMs [14], the omission of core loss leads to considerable calculation inaccuracies, limiting its applicability in high-speed and high-torque/power-density PMSMs. While some researchers, such as Hu *et al*. [15] and Ito *et al*. [16] have attempted core loss modeling within the ECMs, modern PMSMs are extensively employed in variable-speed scenarios, and the single-valued equivalent core loss resistance model cannot accurately predict core loss across a wide range of speeds and loads. Furthermore, the existing ECM structural configurations face challenges in faithfully simulating the rotational magnetization behaviors of core materials.

For the controller part, numerous control methods, including field-oriented control (FOC) [17], direct torque control (DTC) [18], and model predictive control (MPC) [19], have been developed and optimized at the controller level. However, they have seldom been integrated with motor design optimization, such that the desired overall system performance and efficiency cannot be guaranteed. In summary, loss minimization control based on mathematical models, in addition to motor topology optimization, is a highly effective method to enhance the drives' efficiency. It considers multiple types of losses, in contrast to the maximum torque per ampere (MTPA) method, which only addresses copper loss. Moreover, it is more computationally efficient, without the need for convergence requirements, making it readily implementable in controllers without additional hardware demands [20]. However, most mathematical models for loss control in PMSMs may not fully address core losses or control-related losses.

The effectiveness of system-level performance optimizations depends highly on the accuracy of the developed models and the efficiency of the optimization strategies employed. For the optimization models, multi-objective optimization is quite suitable for optimizing PMSM drive systems as they typically involve multiple performance metrics, like efficiency, torque, response time, current waveform quality, cost, and reliability [21]. Furthermore, these metrics are often interrelated and may present trade-offs and conflicts. Several intelligent algorithms, like multi-objective genetic algorithm (MOGA) [22], nondominated sorting genetic algorithm (NSGA) and NSGA II [23], and multi-objective particle swarm optimization (MPSO) [24], effectively address non-inferior Pareto optimums. Despite their global optimization advantages and robustness, their application in electric drive system design optimization is hindered by limited calculation efficiency, particularly in handling high-dimensional finite element models (FEMs). A novel multi-level optimization strategy can be explored to overcome these challenges with enhanced optimization for conflicting parameters.

In summary, this paper aims to present a system-level design optimization strategy for PMSM drive systems using an improved ECM-based loss minimization control method, targeting to maximize the torque and efficiency, while minimizing the torque ripple and speed overshoot. The critical contributions are manifested as follows.

(1) An efficient system-level design optimization scheme for PMSM drive systems, emphasizing efficiency improvement, is proposed. Firstly, an improved ECM-based loss minimization control considering the losses in both motor and control units, is integrated into the scheme for not only simplifying optimization process, but also better-ensuring efficiency improvement. Moreover, rather than focusing on individual components, this paper takes a comprehensive view of the entire system, allowing full concern of complex interactions between motor and controller, ensuring that all elements work in synergy to achieve enhanced overall system performance.

(2) An advanced ECM loss model that accurately predicts the core losses in PMSM drive systems under both no-load and load conditions is developed. The improved model with updated topology considers magnetic saturation and incorporates variable equivalent resistances for hysteresis, eddy current and anomalous losses, together. Moreover, based on the proposed ECM, a system-level loss model of PMSM drive system is established for the loss minimization control and thus the optimization scheme, where high-order formulas and radical calculations can be iteratively solved online by a numerical approach.

(3) A multi-level optimization strategy is introduced to solve the multi-objective optimization model. While significantly decreasing computation time, the Kriging models and NSGA-II algorithms are used to optimize the parameters at each level, and the Pearson sensitivity approach is applied to prioritize labeling. Compared to traditional solving schemes, the proposed strategy can search for optimal solutions with reduced computational burden, enhancing the solving accuracy and efficiency.

(4) The presented equations and hypotheses are all validated by extensive computations, simulations, and experiments conducted on an EV platform with an interior PMSM (IPMSM) drive system prototype. Moreover, the research gap of implementing loss minimization control in the design optimization of drive systems is filled. Experimental results provide conclusive evidence that the design optimization scheme, leveraging the loss minimization control method based on the developed system-level loss model, assures optimal overall system performance and enhanced system efficiency.

The remainder of this paper is organized as follows. Section II presents the design principles of the improved loss minimization control method, encompassing the proposed ECM model and the system-level loss model. In Section III, the multi-level solving strategy for the multi-objective optimization model is introduced. Section IV outlines the numerical and experimental results, showcasing the optimal solutions and performances, followed by the conclusions in Section V.

II. Improved Loss Minimization Control

A. System-level loss model

Efficiency/loss, regarded as a pivotal factor, holds significant influence on optimal solutions and demands precise modeling. Considering that the electrical loss of control units also plays a decisive role in system efficiency, the system-level loss model for a specific PMSM drive system is formulated as follows.

$$P_{total} = P_{Cu} + P_{Fe} + P_{Inv} \tag{1}$$

where P_{Cu}, P_{Fe}, and P_{Inv} are the motor copper loss, motor core loss and inverter loss, respectively.

The losses in a PMSM can be categorized as copper, core loss, mechanical, and additional losses. Among them, the non-

dominant mechanical and additional losses are both very small relative to the total motor loss and they are difficult to measure and control [1], [15]. Thus, only controllable electromagnetic losses (core and copper losses) are considered. For the control side, electrical losses in control units such as detection and control circuits, as well as the inverter, also impact system efficiency to some extent. For most common applications, like EVs, the losses in sensors and control circuits are negligible [1], [6], and therefore P_{inv} is primarily considered in this paper.

B. Equivalent circuit model of PMSM

In this paper, an improved ECM is proposed for PMSMs. As shown in Fig. 1, the upgraded model incorporates three variable equivalent resistances (R_h, R_e, R_{an}) in parallel to the back electromotive force (EMF) in the q-axis circuit to separately represent the hysteresis loss, eddy current loss, and anomalous loss. This placement enables the resistances to vary with frequency and hold a precise analysis of core loss components with respect to working speed through parameter identification. Moreover, to describe additional iron losses caused by the load current, an equivalent resistor R_i is employed in parallel with the electromotive force in the synchronous reactance induced by the armature current in d- and q-axis, through which the PWM high frequency harmonics and the magnetic saturation effects caused by the load currents can all be considered.

According to the proposed ECM, mathematical models are employed to derive equivalent circuit representations of d- and q-axis voltages and currents.

$$\begin{cases} V_d = (R_s + pL_d)I_d - \omega_e L_q I_{mq} \\ V_q = (R_s + pL_q)I_q + \omega_e L_d I_{md} + \omega_e \psi_f \end{cases} \tag{2}$$

and

$$\begin{cases} I_d = I_{cid} + I_{md} \\ I_q = I_{ciq} + I_{miq} = I_{can} + I_{ce} + I_{ch} + I_{mq} \end{cases} \tag{3}$$

where V_d and V_q represent the d- and q-axis terminal voltages, L_d and L_q are the d- and q-axis inductances. Ψ_f, Ψ_d, and Ψ_q stand for the PM and d-axis, q-axis flux linkages. R_s is the resistance of armature winding, ω_e the rotor speed in electrical angular frequency, and p the differential operator (=d/dt). I_d and I_q denote the d- and q-axis armature currents, I_{cid} and I_{ciq} are the d- and q-axis load core loss currents, I_{md}, I_{miq}, and I_{mq} are the d- and q-axis magnetizing currents, and I_{can}, I_{ce}, and I_{ch} are the currents flowing through the resistances R_{an}, R_e, and R_h.

The electromagnetic torque T_{em} can be determined by the following equation, where n_p is the number of pole pairs.

$$T_{em} = \frac{3}{2} n_p \left(\psi_d I_q - \psi_q I_d\right) = \frac{3}{2} n_p [\psi_f + (L_d - L_q) I_d] I_q \tag{4}$$

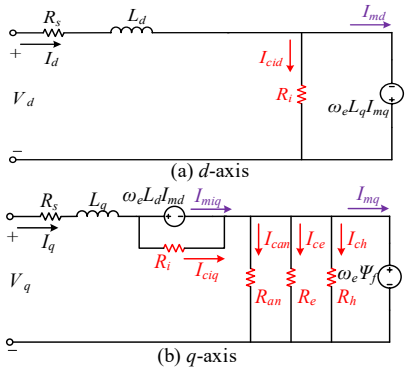

Fig. 1. Improved equivalent circuit considering core loss resistances.

Using (5), the ECM allows for the estimation of the copper loss P_{Cu}, no-load core loss P_{Fe_N}, and load core loss P_{Fe_L}.

$$\begin{cases} P_{Cu} = \frac{3}{2} R_s (I_d^2 + I_q^2) \\ P_{Fe\_N} = \frac{3}{2} (R_{an} I_{can}^2 + R_e I_{ce}^2 + R_h I_{ch}^2) \\ P_{Fe\_L} = \frac{3}{2} \left\{ (R_{an} I_{can}^2 + R_e I_{ce}^2 + R_h I_{ch}^2) + [R_i (I_{cid}^2 + I_{ciq}^2)] \right\} \end{cases} \tag{5}$$

The inverter is a critical component that converts DC power into AC power to drive the motors. During this process, some losses occur due to the switching operations and current flow in the electronic components. Thus, the inverter losses can usually be calculated with switching loss and conduction loss.

$$P_{Inv} = m_1 I_{rms} + m_2 {I_{rms}}^2 \tag{6}$$

where m_1 and m_2 are the inverter loss coefficients that depend on the specific inverter design, topology, and operating conditions. I_{rms} is the magnitude of inverter output current, and

$$I_{rms} = \sqrt{I_d^2 + I_q^2} \tag{7}$$

Then, combining (1), (5), (6) and (7), the system-level loss model for a PMSM drive system is obtained as (8). Given that the no-load losses can also be calculated using (8), this paper focuses solely on presenting the system-level loss model under load conditions.

$$\begin{aligned} P_{total\_L} = {} & \frac{3}{2} R_s (I_d^2 + I_q^2) + \frac{3}{2} (R_{an} I_{can}^2 + R_e I_{ce}^2 + R_h I_{ch}^2) \\ & + \frac{3}{2} [R_i (I_{cid}^2 + I_{ciq}^2)] + m_1 \sqrt{I_d^2 + I_q^2} + m_2 (I_d^2 + I_q^2) \end{aligned} \tag{8}$$

C. Loss minimization control

Based on (8), a revised loss minimization control method is synthesized to improve the drive system efficiency, in which the relationships between T_{em}, I_d and I_q are derived to minimize the system losses. Meanwhile, the currents I_{cid}, I_{ciq}, I_{can}, I_{ce}, and I_{ch} need to be eliminated or replaced for the implementation of loss minimization control.

For eliminating I_{can}, I_{ce} and I_{ch}, based on Fig. 1 (b), the power loss in R_h, R_e and R_{an} can also be calculated via:

$$\begin{cases} P_{Fe\_N} = \frac{3(\omega_e \psi_f)^2}{2} C_{Fe} \\ C_{Fe} = \frac{1}{R_{an}} + \frac{1}{R_e} + \frac{1}{R_h} \end{cases} \tag{9}$$

where C_{Fe} donates the equivalent core loss conductance.

Also, according to the circuit principles shown in Fig. 1, the current equation of (3) can be updated as:

$$\begin{cases} I_d = I_{cid} + I_{md} = I_{md} - \frac{\omega_e L_q I_{mq}}{R_i} \\ I_q = I_{ciq} + I_{miq} = I_{mq} + C_{Fe} \omega_e \psi_f \end{cases} \tag{10}$$

Then, the unknown variables I_{md} and I_{mq} can be derived as:

$$\begin{cases} I_{md} = I_d + \frac{\omega_e L_q}{R_i} (I_q - C_{Fe} \omega_e \psi_f) \\ I_{mq} = I_q - C_{Fe} \omega_e \psi_f \end{cases} \tag{11}$$

And

$$\begin{cases} I_{cid} = -\frac{\omega_e L_q I_{mq}}{R_i} = -\frac{\omega_e L_q (I_q - C_{Fe} \omega_e \psi_f)}{R_i} \\ I_{ciq} = \frac{\omega_e L_d I_{md}}{R_i} = \frac{\omega_e L_d}{R_i} \cdot \left[I_d + \frac{\omega_e L_q}{R_i} (I_q - C_{Fe} \omega_e \psi_f) \right] \end{cases} \tag{12}$$

In combination with (8), (9) and (12), the system-level loss model with respect to I_d and I_q can thus be calculated via:

$$
\begin{aligned}
P_{total\_L} &= \frac{3}{2}R_s(I_d^2+I_q^2)+\frac{3(\omega_e\lambda_f)^2}{2}C_{Fe} \\
&+\frac{3\left[\omega_e L_q(I_q-C_{Fe}\omega_e\psi_f)\right]^2}{2R_i} \\
&+\frac{3\left[\omega_e L_d R_i I_d+\omega_e^2 L_d L_q(I_q-C_{Fe}\omega_e\psi_f)\right]^2}{2R_i^3} \\
&+m_1\sqrt{I_d^2+I_q^2}+m_2(I_d^2+I_q^2)
\end{aligned} \tag{13}
$$

To simplify the following calculation, we define:

$$
\begin{cases}
a_1=\dfrac{3\left(\omega_e L_d\right)^2+R_s R_i}{2R_i};a_2=\dfrac{3R_s R_i^3+\left(\omega_e L_q R_i\right)^2+\left(\omega_e^2 L_d L_q\right)^2}{2R_i^3} \\
a_3=\dfrac{3C_{Fe}\omega_e\psi_f\left[\left(\omega_e^2 L_d L_q\right)^2-\left(\omega_e L_q R_i\right)^2\right]}{R_i^3} \\
a_4=\dfrac{-3C_{Fe}\psi_f\omega_e^4 L_d^2 L_q}{R_i^2};a_5=\dfrac{3\omega_e^3 L_d^2 L_q}{R_i^2} \\
a_6=\dfrac{3C_{Fe}\omega_e^2[\lambda_f^2 R_i^3+C_{Fe}\omega_e^2(\psi_f L_q R_i)^2+C_{Fe}\omega_e^4(\psi_f L_d L_q)^2]}{2R_i^3}
\end{cases} \tag{14}
$$

Then, by substituting (4) and (14) into (13) to eliminate I_q, the system-level loss model of a PMSM drive system considering load loss can be expressed with:

$$
\begin{aligned}
P_{total\_L} &= (a_1+m_2)I_d^2+(a_2+m_2)\left\{\frac{2T_{em}}{3n_p[\psi_f+(L_d-L_q)I_d]}\right\}^2 \\
&+\frac{2a_3T_{em}}{3n_p[\psi_f+(L_d-L_q)I_d]}+a_4I_d+\frac{2a_5T_{em}I_d}{3n_p[\psi_f+(L_d-L_q)I_d]} \\
&+m_1\sqrt{I_d^2+\left\{\frac{2T_{em}}{3n_p[\psi_f+(L_d-L_q)I_d]}\right\}^2}+a_6
\end{aligned} \tag{15}
$$

As the minimum loss control of an electric motor is usually targeted towards load rather than no-load condition in practice, and hence (15) is used for the control law derivation. As seen, the total power loss is a function related to I_d, ω_e and T_{em}, with known parameters like inductance, resistance, PM flux linkage, and number of pole pairs. During steady-state operation, the losses in PMSMs mainly arise from resistances and core losses. By employing a good control strategy, it is possible to minimize these losses and achieve high efficiency in practical applications. During transient operation, like start-up, acceleration, deceleration, or sudden load changes, the motor parameters experience instantaneous variations. In such situations, the control becomes complex, and the transient loss is challenging to estimate and control accurately. Therefore, in the paper, the PMSM drive system working in steady-state is primarily investigated.

In steady-state operation, ω_e and T_{em} can be taken as fixed, and the power loss is only related to I_d. That is, if $\mathrm{d}P_{total\_L}/\mathrm{d}I_d = 0$ is satisfied, the minimum loss of PMSMs can be realized. Then, based on (15), making $\mathrm{d}P_{total\_L}/\mathrm{d}I_d = 0$, one has:

$$
\begin{aligned}
&\frac{m_1\left\{2I_d-\dfrac{4(L_d-L_q)T_{em}}{9n_p^2\left[\psi_f+(L_d-L_q)I_d\right]^3}\right\}}{2\sqrt{I_d^2+\dfrac{2T_{em}}{9n_p^2\left[\psi_f+(L_d-L_q)I_d\right]^2}}}-\frac{4T_{em}^2(L_d-L_q)(a_4+m_2)}{9n_p^2\left[\psi_f+(L_d-L_q)I_d\right]^3} \\
&+\frac{2T_{em}[a_5\psi_f-a_3(L_d-L_q)]}{3n_p\left[\psi_f+(L_d-L_q)I_d\right]^2}+2(a_1+m_2)I_d+a_4=0
\end{aligned} \tag{16}
$$

It is seen that (16) is a complicated nonlinear equation about I_d, such that it is very difficult to solve the function $I_d = f(T_{em})$ conveniently to realize the loss minimization control. Thus, for simplifying computation, (16) is further written as:

$$
F(T_{em})=\frac{m_1(2I_d-Z_2T_{em})}{2\sqrt{I_d{}^2+Z_3T_{em}}}+Z_4T_{em}^2+Z_5T_{em}+Z_1=0 \tag{17}
$$

where

$$
\begin{cases}
Z_1=2(a_1+m_2)I_d+a_4 \\
Z_2=\dfrac{4(L_d-L_q)}{9n_p^2\left[\psi_f+(L_d-L_q)I_d\right]^3} \\
Z_3=\dfrac{2}{9n_p^2\left[\psi_f+(L_d-L_q)I_d\right]^2} \\
Z_4=-\dfrac{4(L_d-L_q)(a_4+m_2)}{9n_p^2\left[\psi_f+(L_d-L_q)I_d\right]^3} \\
Z_5=\dfrac{2[a_5\psi_f-a_3(L_d-L_q)]}{3n_p\left[\psi_f+(L_d-L_q)I_d\right]^2}
\end{cases} \tag{18}
$$

Although (17) looks compact, the non-linearity also leads to difficulty in solving $\mathrm{d}P_{total\_L}/\mathrm{d}I_d = 0$ analytically. Consequently, the numerical Newton–Raphson search method [15] is employed to obtain the solution of (17). The iteration formula is:

$$
T_{em}(k+1)=T_{em}(k)-\frac{F(T_{em}(k))}{F'(T_{em}(k))} \tag{19}
$$

where $T_{em}(k)$ is the approximate solution at the k^{th} iteration.

With the solution of (17), the relationship between T_{em} and I_d is described, based on which the functions $I_d = F(T_{em})$ and $I_q = F(T_{em})$ can also be acquired with the numerical polynomial fitting method.

Therefore, the specific control diagram of the proposed loss minimization control method is given as Fig. 2. In the control scheme, a PI regulator is employed to determine the optimal reference torque T_{em}^* by calculating the difference between the reference and actual speeds. The reference d-axis and q-axis currents (I_d^* and I_q^*) are determined using polynomial functions based on (17)-(19). The PWM controller is then employed to drive the inverter, effectively controlling the PMSM, aiming to enable the motor to operate efficiently and meet the desired loss minimization requirements.

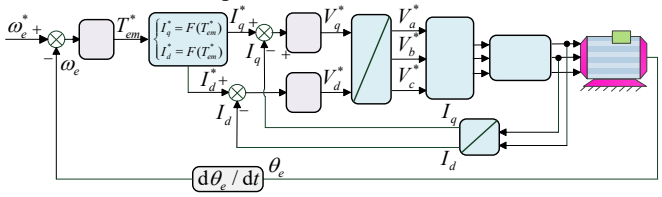

Fig. 2. Block diagram of the proposed loss minimization control method.

III. Multi-objective Optimization With Multi-level Strategy

A. System-level Multi-objective Optimization Method

Several steps are highlighted for system-level design optimization of drive systems with specific PMSMs and controllers.

Step 1: Define system requirements including power, torque, speed, volume, weight, efficiency, etc. in allowed ranges based on the applications.

Step 2: Select the motor and controller types & topology. The interplay between multiphysics and control aspects should be considered. As for EVs, IPMSMs have been increasingly

considered as suitable driving units considering their advantages in terms of efficiency, torque density, and speed range. However, IPMSMs may face challenges when developing high-order loss minimization controllers due to the unequal *d*-axis and *q*-axis inductances and the complex torque expressions.

Step 3: Initially design the motor and controller types & topology, including but not limited to materials, dimensions, electromagnetic, thermal and mechanical characteristics for the motor level, and the control circuits and algorithms for the control level.

Step 4: Establish system-level optimization models to accomplish the performance improvement for the whole system. In practice, the design requirements and optimization objectives of PMSM drive systems are complicated, and engineers prefer multi-objective optimization models to deal with the coupling effects among multiple factors [2].

To guarantee system-level performances of the drive systems, a system-level multi-objective model can be derived by combining the motor and controller design optimization models.

$$\begin{aligned} &\min: f_s(\mathbf{x}_s) = F(f_{mi}, f_{cj}), \quad i = 1,...,P_m; j = 1,...,P_c \\ &s.t. \quad g_{mi}(\mathbf{x}_s) \le 0, \quad i = 1,...,N_m \\ &s.t. \quad g_{ci}(\mathbf{x}_s) \le 0, \quad i = 1,...,N_c \\ &\mathbf{x}_{sl} \le \mathbf{x}_s \le \mathbf{x}_{su} \end{aligned} \tag{20}$$

where $\boldsymbol{x}_s = [\boldsymbol{x}_m, \boldsymbol{x}_c]$ is the decision variable set; $\boldsymbol{x}_m$ and $\boldsymbol{x}_c$ are the parameter vectors of motor level and control level, respectively; $\boldsymbol{x}_{sl}$ and $\boldsymbol{x}_{su}$ are the lower and upper boundaries of $\boldsymbol{x}_s$. f_s is the system-level objective, which is generally a function of motor level objectives f_{mi} and control level objectives f_{ci}; P_m and P_c are the numbers of objectives, while N_m and N_c are the numbers of constraints in motor and control levels, respectively. All the objectives and constraints should be defined in advance according to the requirements/specifications of applications.

Step 5: Optimize the models of the whole electric drive system, including both the motor and controller.

Step 6: Evaluate the whole system's performance.

B. Multi-level Optimization Strategy

The optimization models are often high-dimension problems, which leads to a huge computational cost for FEM and control simulation. To enhance the optimal efficiency, in this paper, an advanced multi-level strategy is utilized [1], [6], which optimizes the model step-by-step by focusing on specific subspaces within the whole parameter space, thereby reducing the overall computational burden while achieving satisfactory optimal accuracy. The flowchart of a multi-level optimization strategy for PMSM drive systems is outlined as Fig. 3. The specific processes are illustrated as follows.

Step 1: With system-level optimization models, sensitivity analysis for all motor parameters will be carried out, by which the initial design space can be divided into several subspaces, i.e., $\mathbf{X}_1$ (highly-significant parameters), $\mathbf{X}_2$ (significant parameters), and $\mathbf{X}_3$ (non-significant parameters). Usually, the controller parameters are assigned in subspace $\mathbf{X}_4$. More subspaces can be defined reasonably if the dimensions are large.

Step 2: Optimize subspace $\mathbf{X}_1$ when parameters in $\mathbf{X}_2$, $\mathbf{X}_3$ and $\mathbf{X}_4$ are fixed. In this study, an optimization process is conducted using approximate models and intelligent algorithms. Initially, a parametric FEM is developed in $\mathbf{X}_1$ for the studied PMSM, and simulations are performed. Then, the results will be utilized to evaluate motor performances and construct an approximate model for reducing computational costs. Subsequently, an intelligent algorithm is employed to find the Pareto solution set of $\mathbf{X}_1$, and the optimal solution is selected for optimizing $\mathbf{X}_2$.

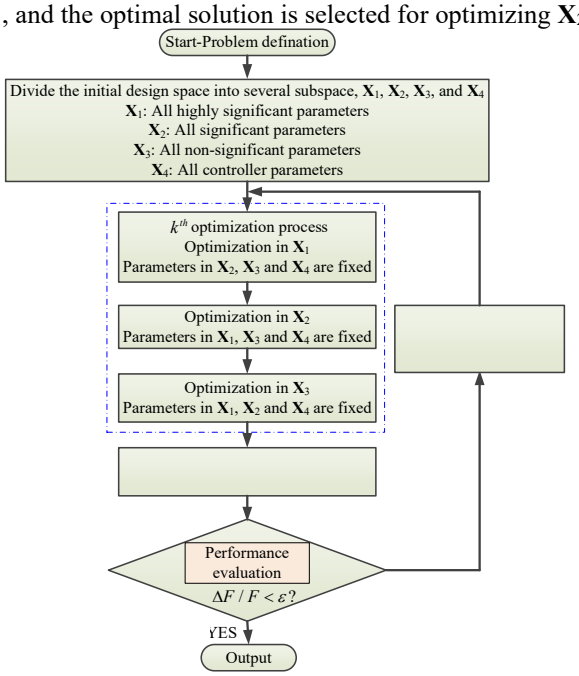

Fig. 3. Flowchart of the proposed multi-level optimization strategy.

Step 3: Optimize subspace $\mathbf{X}_2$ using the optimized parameters in $\mathbf{X}_1$, and the fixed parameters in $\mathbf{X}_3$ and $\mathbf{X}_4$. The same optimization process will be demonstrated.

Step 4: Optimize subspace $\mathbf{X}_3$ using the optimized parameters in $\mathbf{X}_1$ and $\mathbf{X}_2$, and the fixed parameters in $\mathbf{X}_4$. Similarly, after developing the FEM and the optimization model, the Pareto optimal solutions set of $\mathbf{X}_3$ can be obtained with an optimization algorithm.

Step 5: Optimize subspace $\mathbf{X}_4$ using the optimized parameters in $\mathbf{X}_1$, $\mathbf{X}_2$ and $\mathbf{X}_3$, the similar optimization process is carried out.

Step 6: Performance evaluation for PMSM drive systems with the optimal parameters. Continuously monitor the evolution of objective function F, if the relative error, defined as the changing rate of objective function $\Delta F/F$ in two consecutive iterations, is below a pre-determined threshold ε, end the iteration process and generate the optimized results or the Pareto front. Otherwise, update the parameters in $\mathbf{X}_2$, $\mathbf{X}_3$ and $\mathbf{X}_4$, and proceed with another iteration following steps 2-6.

C. Optimization Techniques

Approximate models provide an efficient alternative to FEM, reducing computational burden, which express the relationships between objectives and parameters in multi-objective optimization. Among various modeling techniques, such as the response surface model, and radial basis functions model, the Kriging model stands out for its superior handling of local nonlinearities, as it considers both mean trend and variances of responses [1], [4]. In this paper, the Kriging model is utilized and its required parameters are estimated by the software package DACE (Design and Analysis of Computer Experiments) in Matlab.

Multi-objective optimization involves finding solutions that strike a balance among multiple objectives. The Pareto solutions, which represent the best compromises, are obtained using optimization algorithms. Various techniques, such as DEA, NSGA, and its improved version NSGA II, have been applied

to tackle multi-objective optimization problems [1], [4]. Notably, NSGA II stands out as a highly efficient multi-objective evolutionary algorithm and has been widely adopted in solving industrial multi-objective optimization problems. It usually includes two important components, i.e. the non-dominated sorting approach and the crowd comparison operator. More detailed descriptions about the Kriging model and the NSGA II algorithm can be found in [1], [3], [4].

IV. Results and Discussions

A. Example of An IPMSM Drive System

Testing is performed on a 48-slot 8-pole V-type IPMSM prototype designed for EVs to validate the proposed approaches. The specifications are shown in Table I. The FEM model of the prototype and the diagram of the integrated experimental platform are shown in Fig. 4. To clearly show the stator/rotor structure, the cross-section parameters are given as Fig. 5, while 16 key dimensions are rationalized and confined as in Table II. The IPMSM prototype with the FOC controller was manufactured with the parameters after component-level optimization.

TABLE I
SPECIFICATIONS OF THE IPMSM

Parameters	Unit	Value
Rated power	kW	20
Rated speed	rpm	3600
Rated voltage	V	96
Efficiency	%	85
Stator outer radius	mm	100
Rotor inner radius	mm	22.5

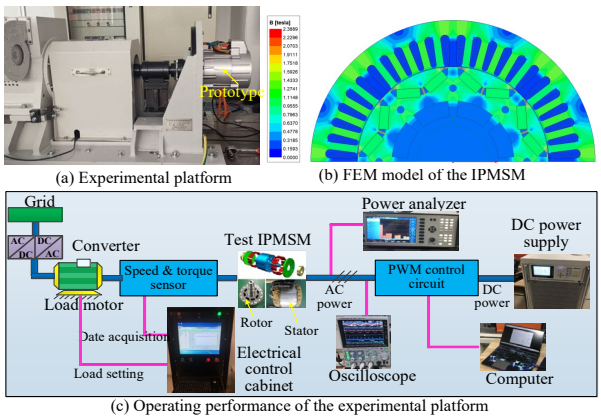

(a) Experimental platform (b) FEM model of the IPMSM

(c) Operating performance of the experimental platform

Fig. 4. Diagram of the integrated experimental platform.

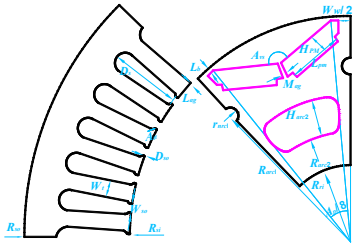

Fig. 5. Structural parameters of the IPMSM.

TABLE II
INITIAL DESIGN PARAMETERS OF THE IPMSM

Parameters	Nom.	Val.	Parameters	Nom.	Val.
Stator inner radius	R_{ro}/mm	60-70	Bridge length	L_b/mm	1
Slot depth	D_s/ mm	17-22	Magnet air	M_{ag}/mm	1.57
Slot opening depth	D_{so}/mm	0.5-1.2	PM height	H_{pm}/mm	6
Slot opening width	W_{so}/mm	1.5-3.5	PM length	L_{pm}/mm	7-9
Tooth width	W_t/ mm	4.2	Pole angle	A_p/ deg	128-136
Tooth tip angle	A_{tt}/ deg	20-45	V-shape an-	A_{vs}/ deg	130-160
Air gap length	L_{ag}/mm	0.5-2	Web width	W_w/mm	5-7

Among these geometric parameters, the tooth width (W_t) and bridge length (L_b) are crucial for stator/rotor structural strength and magnetic flux leakage. While smaller values of W_t, L_b and magnet air gap (M_{ag}) can lead to better electromagnetic performance during electromagnetic finite element optimization, they cannot be too small due to stator and rotor mechanical strength limitations as well as over-saturation. The PM height (H_{pm}) is essential for PMs' demagnetization performance. A relatively small H_{pm} might lead to motor demagnetization, reducing motor reliability. Finally, the remaining ten motor parameters and the six PI gains for speed, d-axis and q-axis currents control, shown in Fig. 2, are considered as the optimization decision variables.

There are a number of operation requirements of an EV drive system, concerning high steady and dynamic performance, cost, energy saving, environment, comfortability, etc. In this study, the optimization model is defined as:

$$\min:\begin{cases} f_1(\mathbf{X}_S) = -T_{\max} \\ f_2(\mathbf{X}_S) = T_{rip} \\ f_3(\mathbf{X}_S) = n_{os} \end{cases} \quad s.t.:\begin{cases} 0.85-\eta_m \le 0; 150-T_{\max} \le 0 \\ sf-0.8 \le 0; J_C - 6 \le 0 \\ n_{os}-0.1 \le 0; T_{rip}-0.1 \le 0 \end{cases} \tag{21}$$

where T_{max} is the maximum torque, n_{os} the speed overshoot, and T_{rip} the torque ripple at the rated operating point. $\boldsymbol{X}_S$ is the designed decision variables in the system level, η_m the motor efficiency, sf the slot filling factor, and J_C the current density of stator winding. It should be noted that, in this paper, the maximum efficiency goal is achieved through the proposed loss minimization control for not only further simplifying the optimal dimensions but also reducing the system-level loss.

As given in (21), it is a multi-objective optimization model which can achieve a balanced performance comprehensively with only Pareto optimal solutions instead of the single solution set. Therefore, a selection criterion is defined as (22), by which the candidate point can be chosen from the Pareto solutions for the iterations. The power loss is calculated through FEM.

$$\min: F_{cri} = \alpha_1 \frac{T_{\max\_ini}}{T_{\max}} + \alpha_2 \frac{P_{total}}{P_{total\_ini}} + \alpha_3 \frac{T_{rip}}{T_{rip\_ini}} + \alpha_4 \frac{n_{os}}{n_{os\_ini}} \tag{22}$$

where the subscript *ini* represents the parameters under the initial design. α_1, α_2, α_3 and α_4 are all weighting factors. Through extensive consultations, along with rich literature references, it is concluded that the torque and efficiency metrics are slightly more important than the latter two indicators, especially for EV drive systems [2], [5]. Consequently, the four weights are assigned as 0.3, 0.3, 0.2 and 0.2, respectively. After obtaining the Pareto solutions, the single objective (22) can be used to choose the candidate points.

B. Sensitivity Analysis

The Pearson sensitivity analysis method is well-suited for assessing the relationships between objectives and decision variables efficiently, even when dealing with a large number of parameters. Moreover, in practice, we need to estimate the sample standard deviations $s_{\mathbf{x}}$ and $s_{\mathbf{y}}$ to obtain the sample Pearson correlation coefficient with [4], [6]:

$$\rho(x_i, y_i) = \frac{\sum x_i y_i - n\overline{\mathbf{xy}}}{(N_s-1)s_{\mathbf{x}}s_{\mathbf{y}}} = \frac{N_s\sum x_i y_i - \sum x_i \sum y_i}{\sqrt{N_s\sum x_i^2 - (\sum x_i)^2}\sqrt{N_s\sum y_i^2 - (\sum y_i)^2}} \tag{23}$$

where x_i are the design parameters, y_i are the optimization objectives, and N_s is the sample size.

In addition to the four non-optimized parameters mentioned above, the Pearson correlation coefficients of the remaining ten motor parameters on the objectives are calculated, as given in Fig. 6. As shown, the air gap length (L_{ag}), PM length (L_{pm}), web width (W_w) and stator inner radius (R_{ro}) exhibit significant influences on the majority of objectives. The absolute average Pearson correlation coefficients for these variables are all greater than 0.85. The pole angle (A_p), slot depth (D_s) and slot opening width (W_{so}) have notably high Pearson correlation coefficients, averaging at 0.779, 0.776 and 0.782, respectively, while other parameters show values below 0.6. In this case, the subsections are distinguished as $\mathbf{X_1} = [x_1, x_2, x_3, x_4] = [L_{ag}, L_{pm}, W_w, R_{ro}]$, $\mathbf{X_2} = [x_5, x_6, x_7] = [A_p, D_s, W_{so}]$, and $\mathbf{X_3} = [x_8, x_9, x_{10}] = [D_{so}, A_{tt}, A_{vs}]$.

On the other hand, considering that motor parameters are intrinsic to the design and construction, which may affect steady-state behaviors, but cannot be adjusted during operation, the six PI gains are categorized under the fourth level $\mathbf{X}_4$, optimizing responses to changing work conditions. The precedence of optimizing the motor parameters before the controller parameters is grounded in the fundamental influence of motor characteristics on the overall drive system performance. By prioritizing the optimization of motor parameters initially, a robust foundation can be laid for subsequent tuning of controller parameters. This sequential optimization strategy, rooted in empirical observations of motor drive systems, ensures harmonious coordination between optimized motor characteristics and control algorithms, thus enhancing the system's overall performance [1], [5].

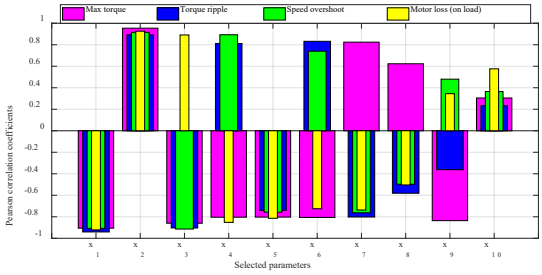

Fig. 6. Sensitivities analysis results of the selected motor parameters.

C. Verification of the Loss Minimization Control

To demonstrate the effectiveness and accuracy of the proposed ECM, especially considering the PWM high frequency harmonics, a series of experiments are conducted, in which the iron loss of the IPMSM prototype shown in Fig. 4 is measured, and then compared with the values obtained by the FEM, the improved analytical model in [9], and the proposed ECM. The specific information for acquiring the measured iron loss values can be found in [9]. It should be noted that, for determining the equivalent resistances in the ECM, the core loss coefficients are firstly obtained by curve fitting the actual no-load core loss data under different working speeds. Furthermore, it can also be deduced that R_h is a linear function of motor speed n, R_e is a constant, and R_{an} is proportional to the square root of n. In this case. we can finally acquire that $R_h = 0.685n\ \Omega$, $R_e = 563.71\ \Omega$, and $R_{an} = 2.1153n^{0.5}\ \Omega$. To determine the value of R_i, the motor iron losses under various load currents and speeds are figured out. Assuming that the additional iron loss is proportional to the square of the load current and the motor speed, then, as for designs of the prototype, R_i can be calculated as 106.4069 Ω based on the curve-fitted relationships between the load-caused additional iron loss versus load current and speed.

Finally, the comparative results of iron losses under both no-load and load (rated input current) conditions are obtained as Fig. 7. As shown, under no-load condition, as the resistances including R_h, R_e, R_{an} are all fitted with actual loss data, the iron loss values predicted with the proposed ECM are relatively close to those measured with the IPMSM prototype at different working speeds. The maximum and absolute average errors are all less than 2%, compared to the measured iron loss values, which are smaller than the FEM results and accounting only around one third of the method in [9]. Under load condition, as seen from Fig. 7(b), because the model in [9] has considered coupling effects of multiphysics factors like harmonics, temperature rise and mechanical stress, it can predict the load iron loss with high accuracy (within 5.22%), especially in relatively low speed operating range. Moreover, the iron loss calculated with the proposed ECM also shows satisfactory prediction stability and accuracy. The maximum error is only 5.08%, while the absolute average error accounts for 3.74%, which are only around 40% of the errors for the numerical FEM. All the results well-verify the satisfactory performance of the proposed EMC for predicting no-load and load iron losses of IPMSMs.

Considering that the performance of the proposed loss minimization controller plays a crucial role in the following design optimization of the PMSM drive system, three groups of comparative experiments are demonstrated, in which the control performance of the proposed controller was deeply analyzed and compared with those obtained with traditional FOC and MTPA methods. The results concerning loss indicators are all given as Fig. 8.

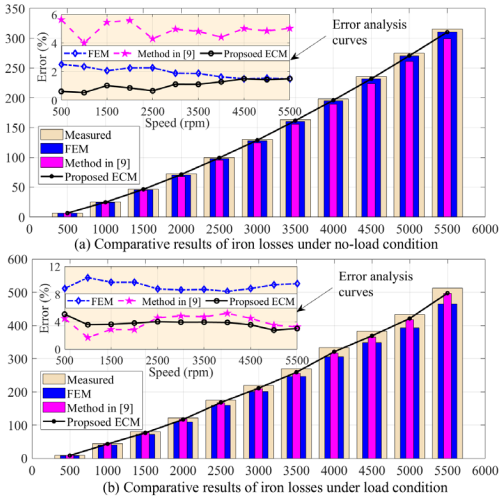

Fig. 7. Comparative results of iron losses obtained with various models.

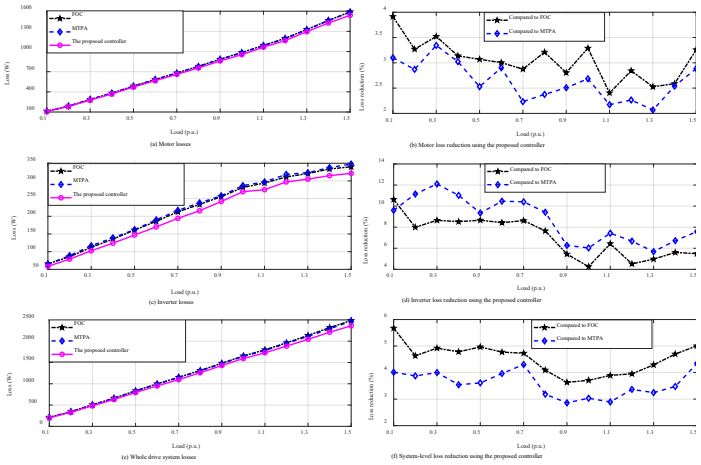

Fig. 8. Comparative results of loss performances with various controllers.

As shown, under different working loads, using the proposed loss minimization controller, the PMSM drive system has the minimum motor loss, inverter loss and whole drive system loss. Compared to FOC, the motor, inverter and system losses can be evenly reduced by about 3.05 %, 7.06% and 4.52%, respectively, while the three loss indicators are reduced by about 2.63%, 8.66% and 3.58%, compared to the MTPA method. The superiority of the proposed controller in efficiency improvement is verified.

D. Optimization Results

As illustrated, the Kriging model is utilized to approximate the IPMSM drive system model, while the NSGA-II optimization algorithm is selected for the solving process in each level. FEM and Matlab/Simulink are employed to calculate the system performances such as torque, speed, and torque ripple at rated speed. After three iterations, the convergence criterion of F_{cri} is triggered, and the Pareto optimal solutions of each subspace under different iterations are expressed in Figs. 9 to 11.

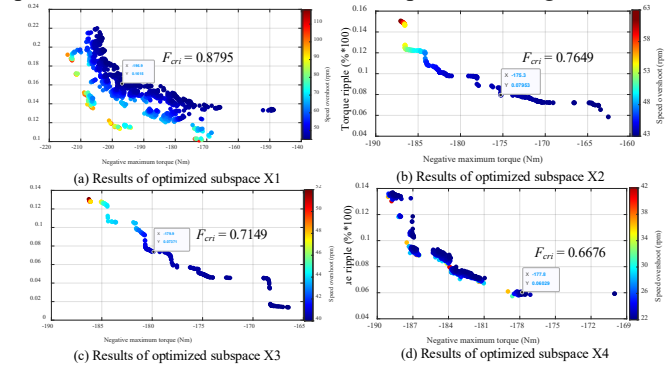

Fig. 9. Pareto optimal solutions of iteration 1.

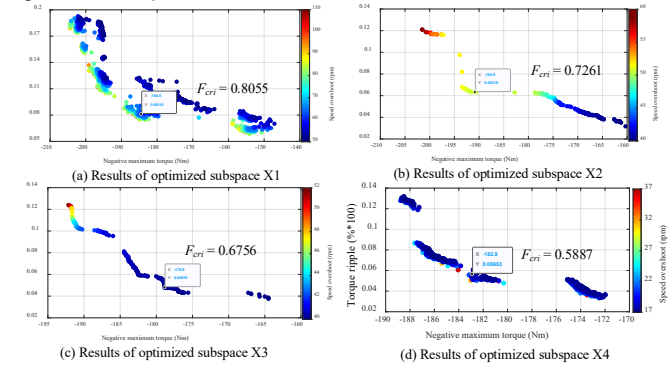

Fig. 10. Pareto optimal solutions of iteration 2.

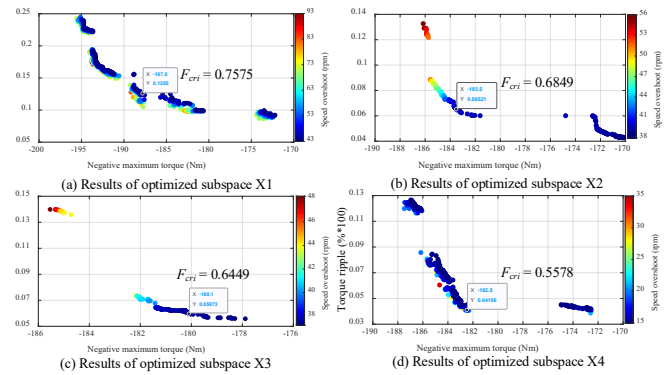

Fig. 11. Pareto optimal solutions of iteration 3.

In subspace $\mathbf{X}_1$ with 4 dimensions, $6^4 = 1296$ FEM samples are generated for the optimization. As shown in Fig. 9(a), the proposed approach can obtain a series of Pareto solutions after the first level optimization. And the result with a minimum F_{cri} defined in (26) will be sent to the second level optimization of subspace $\mathbf{X}_2$, in which $6^3 = 216$ samples are collected. Similarly, based on the selected optimal solution in $\mathbf{X}_1$ and $\mathbf{X}_2$, the optimization of subspaces $\mathbf{X}_3$ and $\mathbf{X}_4$ are accomplished using $6^3 = 216$ and $3^6 = 729$ samples, respectively. Thus, the total number of samples when using the proposed multi-level strategy is only 2457, much smaller than those in single-level optimization with 16 dimensions (about 5^{16}), which can undoubtedly reduce the computing costs greatly. Taking Fig. 9 as an example for analysis, and comparing Figs. 9(a) and (b), it is seen that the torque ripple is reduced greatly, while comparing Figs. 9(c) and (d), the speed overshoot is suppressed, which indicates that optimization of subspace $\mathbf{X}_2$ and $\mathbf{X}_4$ is better in reducing the torque ripple and speed overshoot, respectively. The unanimous conclusion can also be obtained from Figs. 10 and 11.

The comparative results of each iteration are listed in Table III. As the iteration number increases, most performance metrics in the used IPMSM drive system are optimized. Compared to the initial scheme, the maximum torque is promoted from 160.5 to 182.5 N·m, while the torque ripple is reduced from 15.5% to 4.2%, and the speed overshoot is reduced from 75 to around 18.2 rpm. Moreover, the objective value F_{cri} also shows improvement, decreasing from 0.6676 to 0.5578, indicating that the final optimization results bring about the best balance in performance for the drive system. However, it is observed that during the iteration process, the maximum torque experiences a slight decrease, which may be a result of striking a balance among different objectives. Furthermore, the system's losses are maintained at around 1600 W, remaining relatively low due to the benefits of the proposed loss minimization control.

TABLE III
OPTIMIZATION RESULTS OF EACH ITERATION

NOM.	UNIT	INITIAL	ITERATION1	ITERATION2	ITERATION3
D_s	mm	17-22	19.8	20.2	19.9
L_{ag}	mm	0.5-2	1.67	0.89	1.63
W_{so}	mm	1.5-3.5	2.78	2.16	1.97
R_{ro}	mm	60-70	69.5	67.6	68.8
L_{pm}	mm	7-9	7.5	8.2	8.3
A_p	deg	128-136	128	128.1	128.1
W_w	mm	5-7	6.6	6.8	6.9
D_{so}	mm	0.5-1.2	0.72	0.79	0.70
A_{tt}	deg	20-45	27.4	26.1	24.7
A_{vs}	deg	130-160	153	155	145

C_{P1}	---	0.1	1.25	1.36	1.38
C_{P2}	---	0.1	0.47	0.42	0.42
C_{P3}	---	0.1	0.95	1.15	1.16
C_{I1}	---	0.05	0.16	0.11	0.13
C_{I2}	---	0.05	0.04	0.04	0.02
C_{I3}	---	0.05	0.35	0.64	0.70
T_{max}	Nm	160.5	177.8	182.9	182.5
T_{rip}	%	15.5	6.0	5.7	4.2
n_{os}	rpm	75	24.6	19.5	18.2
P_{total}	W	2500	2115	1666	1594
F	---	1.00	0.6676	0.5887	0.5578

The computational costs for each subspace are listed in Table IV. The optimization dimension is greatly reduced by using the multi-level strategy and loss minimization controller. Most computational costs (less than 12 hours in each subspace, and less than 24 hours in total) are used for generating samples in simulations, while only several seconds are taken for solving models. The computing time is greatly reduced compared to one-level optimization with 16 dimensions (5^{16} samples).

TABLE IV
COMPARATIVE OF COMPUTATIONAL COSTS FOR EACH SUBSPACE

ISSUES	TIME $\mathbf{X}_1$	TIME $\mathbf{X}_2$	TIME $\mathbf{X}_3$	TIME $\mathbf{X}_4$
Simulation sample	11.26 h	2.47 h	3.19 h	6.72 h
Model solving	39.93 s	1.92 s	2.77 s	19.24 s

E. Performance Validation

To verify the effectiveness of the proposed system-level optimization approaches utilizing the improved ECM-based loss minimization controller, the torque performances including the maximum and cogging torques, of the final optimized IPMSM drive system are analyzed and compared with those in the initial design point and prototype with the component-level optimized parameters and FOC, given as Figs. 12 to 13, respectively.

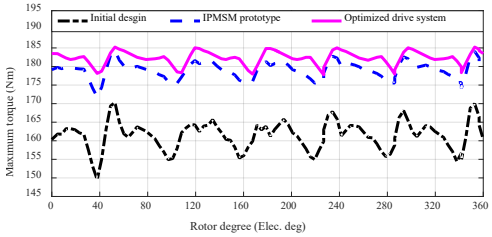

Fig. 12. Comparative results of maximum torque.

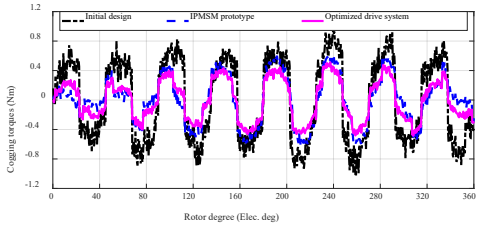

Fig. 13. Comparative results of cogging torque.

As shown in Fig. 12, the maximum torque of the optimized drive system is about 182.5 N·m, 2.5% and 13.7% larger than that of the prototype (178 N·m) and the initial design scheme (160.5 N·m). Moreover, the torque ripple is reduced to 4.17%, only about one third of that in the initial drive system. As illustrated in Fig. 13, the optimized cogging torque curve outperforms both the prototype and the initial design. Meanwhile, the maximum cogging torque in the optimized scheme is only 0.51 N·m, about 85% and 60% of the values measured with the prototype and those obtained via initial motor parameters.

Combining with the FEM model and Matlab/Simulink, the comparative results of working speed behaviors are outlined in Fig. 14. As seen, the optimized IPMSM drive system exhibits significantly smaller speed overshoots (less than 1%) compared to the initial and measured systems across the entire speed range. Moreover, the average steady-state errors stay within 0.5% consistently, providing clear evidence of the enhanced dynamic performance achieved by the proposed optimization strategy.

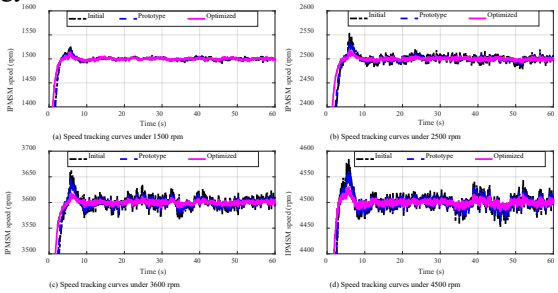

Fig. 14. Comparative results of speed tracking curves.

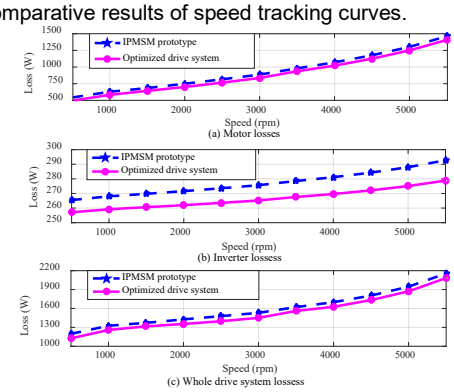

Fig. 15. Comparative results of power losses.

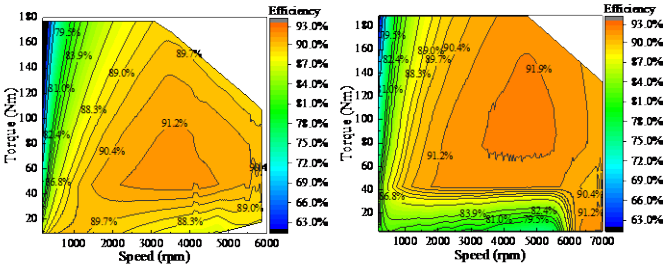

Fig. 16. Comparative results of system-level efficiency map.

Finally, to validate the functions of the proposed loss minimization control method, the motor, inverter and system losses of the optimized PMSM drive system are calculated under rated load condition and compared with those measured using the integrated experimental platform with a FOC control. The results are shown in Fig. 15. Under different working speeds, the optimized IPMSM drive system with the proposed loss minimization control, can effectively reduce the motor loss, and inverter loss by about 5.64% and 3.86%, as well as the system loss by about 4.57%. This is crucial for improving system efficiency with considerable significance. It can also be seen from Fig. 16 that the optimized average system-level efficiency is up to 90.45%, higher than the average value measured with the prototype (87.20%).

V. CONCLUSIONS

This paper presented an improved system-level design optimization strategy for PMSM drive systems used in EVs. Multi-

objectives were considered to achieve an optimal balance performance, and the multi-level scheme was utilized to reduce the computation burden. More importantly, aiming to suppress the electricity costs in the lifecycle, an integrated system-level loss model for the PMSM drive system was developed based on the proposed accurate core loss ECM model. Then, an effective loss minimization control method was synthesized to realize the system efficiency optimization. Comparative experimental and simulation case studies were demonstrated in an IPMSM drive system, by which the effectiveness of the proposed approaches was well verified. The main conclusions are as follows.

1) The proposed loss minimization control method achieved the target of minimizing losses, enhancing overall system efficiency without the necessity for separate optimization levels. The steady-state and dynamic performances are elevated, and both the design space and searching speed can also be enhanced.

2) An optimal solution was selected from Pareto optimal sets with the defined selection criterion. Coupled with the sensitivity analysis and multi-level strategies, the optimization accuracy and efficiency can be guaranteed.

3) Experimental results validated that the optimized drive system realizes promoted performances in all aspects of efficiency, maximum torque, torque ripple and speed overshoot.

The outcomes from this paper may provide a valuable guideline for the design optimization of various drive systems in transportation electrification. Future works will focus on exploring the robustness of the proposed optimization strategy under varying operating conditions and driving scenarios.

REFERENCES

[1] G. Lei, J. Zhu, and Y. Guo, *Multidisciplinary design optimization methods for electrical machines and drive systems*, Berlin, Heidelberg: Springer Berlin / Heidelberg, 2016.

[2] X. Sun, Z. Shi, *et al*., "Driving cycle oriented design optimization of a permanent magnet hub motor drive system for a four-wheel-drive electric vehicle," *IEEE Trans. Transp. Electr.*, vol. 6, no. 3, pp. 1115-1125, 2020.

[3] V. Ghorbanian and D. A. Lowther, "Magnetic and electrical design challenges of inverter-fed permanent magnet synchronous motors," *IEEE Trans. Magn.*, vol. 53, no. 6, pp. 1-4, Jun. 2017.

[4] G. Lei, X. M. Chen, and J. G. Zhu, *et al*., "Multi-objective sequential optimization method for the design of industrial electromagnetic devices," *IEEE Trans. Magn.*, vol. 48, no. 11, pp. 4538-4541, Nov. 2012.

[5] K. Diao, X. Sun, *et al*., "System-level robust design optimization of a switched reluctance motor drive system considering multiple driving cycles," *IEEE Trans. Energy Convers.*, vol. 36, no. 1, pp. 348-357, 2021.

[6] G. Lei, W. Xu, and J. Hu, *et al*., "Multi-level design optimization of a FSPMM drive system by using sequential subspace optimization method," *IEEE Trans. Magn.*, vol. 50, no. 2, pp. 685-688, Feb. 2014.

[7] Z. Tang and B. Akin, "A new LMS algorithm based deadtime compensation method for PMSM FOC drives," *IEEE Trans. Ind. Appl.*, vol. 54, no. 6, pp. 6472-6484, Nov.-Dec. 2018.

[8] E. Dlala, "A simplified iron loss model for laminated magnetic cores," *IEEE Trans. Magn.*, vol. 44, no. 11, pp. 3169-3172, Nov. 2008.

[9] L. Liu, X. Ba, and Y. Guo, *et al*., "Improved iron loss prediction models for interior PMSMs considering coupling effects of multiphysics factors," *IEEE Trans. Transp. Electr.*, vol. 9, no. 1, pp. 416-427, Mar. 2023.

[10] X. Chen, J. Wang, and B. Sen, "A high-fidelity and computationally efficient model for interior permanent-magnet machines considering the magnetic saturation, spatial harmonics, and iron loss effect," *IEEE Trans. Ind. Electron.*, vol. 62, no. 7, pp. 4044-4055, Jul. 2015.

[11] I. Suehiro, T. Mifune, and T. Matsuo, *et al*., "Ladder circuit modeling of dynamic hysteretic property representing excess eddy-current loss," *IEEE Trans. Magn.*, vol. 54, no. 3, pp. 1-4, Mar. 2018.

[12] A. Hemeida, A. Lehikoinen, and P. Rasilo, *et al*., "A simple and efficient quasi-3D magnetic equivalent circuit for surface axial flux permanent magnet synchronous machines," *IEEE Trans. Ind. Electron.*, vol. 66, no. 11, pp. 8318-8333, Nov. 2019.

[13] A. R. Tariq, C. E. Nino-Baron, and E. G. Strangas, "Iron and magnet losses and torque calculation of interior permanent magnet synchronous machines using magnetic equivalent circuit," *IEEE Trans. Magn.*, vol. 46, no. 12, pp. 4073-4080, Dec. 2010.

[14] S. K. Kommuri, Y. Park, and S. B. Lee, "Online compensation of mechanical load defects with composite control in PMSM drives," *IEEE/ASME Trans. Mech.*, vol. 26, no. 3, pp. 1392–1400, Jun. 2021.

[15] D. Hu, W. Xu, and R. Dian, *et al*., "Loss minimization control of linear induction motor drive for linear metros," *IEEE Trans. Ind. Electron.*, vol. 65, no. 9, pp. 6870-6880, Sep. 2018.

[16] S. Ito, T. Mifune, and T. Matsuo, *et al*., "Equivalent circuit modeling of DC and AC ferrite magnetic properties using H-input and B-input play models," *IEEE Trans. Magn.*, vol. 49, no. 5, pp. 1985-1988, May 2013.

[17] Z. Qian, T. Huang, and W. Wang, *et al*., "Torque ripple reduction of PMSM based on modified DBN-DNN surrogate model," *IEEE Trans. Transp. Electr.*, vol. 9, no. 2, pp. 2820-2829, Jun. 2023.

[18] C. Xia, J. Zhao, *et al*., "A novel direct torque control of matrix converter-fed PMSM drives using duty cycle control for torque ripple reduction," *IEEE Trans. Ind. Electron.*, vol. 61, no. 6, pp. 2700-2713, Jun. 2014.

[19] M. Peña, M. Meyer, *et al*., "Model predictive direct self-control for six-step operation of permanent-magnet synchronous machines," *IEEE Trans. Power Electron.*, vol. 38, no. 10, pp. 12416-12429, Oct. 2023.

[20] R. Ni, D. Xu, and G. Wang, *et al*., "Maximum efficiency per ampere control of permanent-magnet synchronous machines," *IEEE Trans. Ind. Electron.*, vol. 62, no. 4, pp. 2135–2143, Apr. 2015.

[21] M. E. Beniakar, A. G. Sarigiannidis, and P. E. Kakosimos *et al*., "Multi-objective evolutionary optimization of a surface mounted PM actuator with fractional slot winding for aerospace applications," *IEEE Trans. Magn.*, vol. 50, no. 2, pp. 665-668, Feb. 2014.

[22] D. K. Lim, D. K. Woo, and H. K. Yeo, *et al*., "A novel surrogate-assisted multi-objective optimization algorithm for an electromagnetic machine design," *IEEE Trans. Magn.*, vol. 51, no. 3, pp. 1-4, Mar. 2015.

[23] Y. Hua, H. Zhu, *et al*., "Multi-objective optimization design of permanent magnet assisted bearingless synchronous reluctance motor using NSGA-II," *IEEE Trans. Ind. Electron.*, vol. 68, no. 11, pp. 10477-10487, 2021.

[24] J. Zhang, H. Wang, *et al*., "Multi-objective optimal design of bearingless switched reluctance motor based on multi-objective genetic particle swarm optimizer," *IEEE Trans. Magn.*, vol. 54, no. 1, pp. 1-13, Jan. 2018.

Lin Liu (S'20) received the B.E. and M.E. degrees in control and computer engineering from North China Electric Power University, Beijing, China, in 2016 and 2019, respectively. She is currently working toward a Ph.D. degree in electrical and data engineering with the University of Technology Sydney (UTS). Her research area includes the design optimization of electrical drive systems.

Youguang Guo (S'02-M'05-SM'06) received the M.E. degree from Zhejiang University, China in 1988, and the Ph.D. degree from University of Technology Sydney, Australia in 2004, all in electrical engineering. He is currently a Full Professor at the School of Electrical and Data Engineering, UTS. His research fields include measurement and modeling of properties of magnetic materials, electrical machine design optimization.

Wenliang Yin (S'17-M'19) received his B.E. degree and Ph.D. degree in power machinery and engineering from North China Electric Power University, Beijing, China, in 2014 and 2019, respectively. He is currently working as a Postdoc Fellow with School of Electrical and Information Engineering, The University of Sydney, Australia. His research interests include technology and equipment of wind power generation system.

Gang Lei (M'14-SM'20) received the M.S. degree and Ph.D. degree in Electrical Engineering from Huazhong University of Science and Technology, China, in 2006 and 2009. He is currently a Senior Lecturer at the School of Electrical and Data Engineering, University of Technology Sydney, Australia. His research areas include electrical machines, multidisciplinary design optimization, industrial big data techniques.

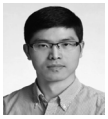

Xiaodong Sun (SM) received the M.Sc. and Ph.D. degrees in control engineering from Jiangsu University, China, in 2008, and 2011, respectively. He is currently a Professor with the Automotive Engineering Research Institute, Jiangsu University. His research interests include electrified vehicles, electrical machines, electrical drives, and energy management.

Jianguo Zhu (S'93–M'96–SM'03) received the Ph.D. degree from the University of Technology, Sydney (UTS), Australia, in 1995, in electrical engineering. He was promoted to a Full Professor in 2004 and a Distinguished Professor of electrical engineering in 2017, UTS. In 2018, he joined The University of Sydney, Australia, as a Full Professor and the Head of the School of Electrical and Information Engineering. His research interests include electromagnetics, magnetic properties, electrical machines and drives, power electronics.